HEAT TRANSFER ENHANCEMENT BY SUSPENDED PARTICLES IN A TURBULENT SHEARLESS FLOW

33RD CONGRESS
OF THE INTERNATIONAL COUNCIL
OF THE AERONAUTICAL SCIENCES
STOCKHOLM, SWEDEN, 4-9 SEPTEMBER, 2022

ICAS 2022 SWEDEN

HEAT TRANSFER ENHANCEMENT BY SUSPENDED PARTICLES IN A TURBULENT SHEARLESS FLOW

Hamid Reza Zandi Pour[1] & Michele Iovieno[1]

[1]Dipartimento di Ingegneria Meccanica e Aerospaziale, Politecnico di Torino

Abstract

Numerical simulations are used to investigate the role of particle inertia and thermal inertia on the heat transfer in a particle-laden turbulent flow. By using the point-particle model, a wide range of Stokes and thermal Stokes number have been simulated in a simple configuration where a temperature discontinuity is introduced in a statistically steady homogeneous and isotropic turbulent flow with a Taylor microscale Reynolds number between 37 and 124. This configuration produces a self-similar evolution of the carrier flow and particle temperature statistics during which the Nusselt number remains constant. Our results show that the maximum contribution by particles to the heat flux is achieved at a Stokes number which increases with the ratio between thermal Stokes and Stokes number, approaching one for very large ratios. Moreover, the maximum increases with the thermal Stokes to Stokes number ratio and, relatively to the convective heat flux, it reduces as the Reynolds number increases.

Keywords: particle-laden flows, turbulence, turbulent mixing, heat transfer

1. Introduction

Particle-laden and droplet-laden turbulent flows are very frequent in nature and in industrial applications and, as such, they have attracted the interest of the scientific community since the pioneering works by Taylor and Richardson and these flows are still an active research area [1, 2]. In the last two decades, the possibility to perform numerical simulations due to the ever increasing high performance computing capabilities has allowed to obtain significant progresses in the understanding of the mechanisms behind the observed phenomenology. Even if up to now a Direct Numerical Simulations (DNS) of a complex flow or a high Reynolds number flow are not be possible, still a significant insight can be obtained from the investigation of simple and idealized archetypal flow configurations. Indeed, turbulent particle-laden flows are a multi-scale and multi-physics phenomenon and many aspects of these flows have not yet fully understood. This is particularly evident when the thermal interaction between the particles and the carrier flow is taken in consideration, because the resulting flow is the outcome of a non-trivial interaction between particle inertia, particle thermal inertia, heat transport, and momentum and heat feedback of the particles on the carrier fluid.

In recent years, many works have considered some aspects of the fluid-particle temperature coupling using direct numerical simulations, mainly within the point-particle approach valid for small sub-Kolmogorov particles, which is a frequent situation in many applications. For example, Zonta et al. [3] investigated a particle-laden channel flow, with the aim to model the modification of heat transfer in micro-dispersed fluids, observing that particle inertia can lead to an increase or decrease of the wall heat flux. Kuerten et al. [4] considered a similar set-up with larger dispersed particles, and observed a stronger modification of the carrier fluid temperature statistics induced by the presence of particles. Zamansky et al. [5] considered turbulence induced by the buoyancy was generated by the heating of particles, analyzing the flow driven by the thermal plumes produced by the heated particles. In such a case, an increase of particle inertia increased the inhomogeneity of the flow and the effects of the fluid-particle coupling were enhanced by the tendency of particles to cluster on the

advected scalar fronts. Kumar et al. [6, 7] examined how the spatial distribution of water droplets in air is affected by large scale inhomogeneities in the fluid temperature and supersaturation fields, considering the transition between homogeneous and inhomogeneous mixing. In this situation, the leading role in the thermal interaction between droplets and air is the release or absorption of the latent heat of evaporation due to the condensation or evaporation of water vapour. Other works, e.g. [8] and [9], considered droplet dynamics at a temperature/humidity interface in the absence of mean shear. Finally, Carbone et al. [10] and Saito et al. [11] have theoretically and numerically investigated the multi-scale aspects of fluid-particle thermal interaction in homogeneous and isotropic turbulence and the modulation of the carrier flow temperature by the particle thermal feedback.
The present work aims to extend such works by investigating the fluid-particle thermal interaction in turbulent mixings in the one-way coupling regime. In particular, we discuss the role of particle inertia and thermal inertia on the heat transfer in the simplest inhomogeneous flow configuration, where heat is transferred between two regions at different temperatures by a statistically homogeneous and isotropic velocity field. We consider that the flow is seeded by a suspension of monodisperse non-buoyant rigid spherical particles, which are assumed to have sub-Kolmogorov size so that the point-particle paradigm can be used. This is an archetypal configuration which can help to highlight the most fundamental consequences of the presence of particles with a finite inertia and thermal inertia. Moreover, it provides a simple benchmark flow to check the parametrization of turbulent transport in Reynolds Averaged equations (RANS) or the subgrid modelling in the Large-Eddy Simulation (LES).

2. Method

2.1 Physical model

In this section we present the governing equations of the physical model which have been used to simulate the dynamics of a particle-laden turbulent flow within the point-particle paradigm. The Navier-Stokes equations for the carrier fluid are

$$\nabla\cdot\boldsymbol{u} = 0, \tag{1}$$

$$\partial_t\boldsymbol{u} + \boldsymbol{u}\cdot\nabla\boldsymbol{u} = -\frac{1}{\rho_0}\nabla p + \nu\nabla^2\boldsymbol{u} + \frac{1}{\rho_0}\boldsymbol{C}_u + \boldsymbol{f}_u, \tag{2}$$

$$\partial_t T + \boldsymbol{u}\cdot\nabla T = \kappa\nabla^2 T + \frac{1}{\rho_0 c_{p0}} C_T, \tag{3}$$

where $\boldsymbol{u}(t,\boldsymbol{x})$ is the fluid velocity, $p(t,\boldsymbol{x})$ is the pressure, $T(t,\boldsymbol{x})$ is the fluid temperature, ρ_0 and c_{p0} are the fluid density and specific heat at constant pressure, ν and κ are the kinematic viscosity and thermal diffusivity, $\boldsymbol{f}_u$ is a forcing term to keep the flow in a statistically steady state and, finally $\boldsymbol{C}_u$ and C_T are the particle momentum and heat feedback (see [10]). The temperature field has been considered a passive scalar, advected by the solenoidal velocity field and subject to the particle thermal feedback in the two-way regime. The dynamics of heavy ($\rho_p \gg \rho_0$) inertial particles, much smaller than any flow scale, is governed by the following equations

$$\frac{\mathrm{d}^2\boldsymbol{x}_p}{\mathrm{d}t^2} = \frac{\mathrm{d}\boldsymbol{v}_p}{\mathrm{d}t} = \frac{\boldsymbol{u}(t,\boldsymbol{x}_p) - \boldsymbol{v}_p}{\tau_p}, \qquad \frac{\mathrm{d}\theta_p}{\mathrm{d}t} = \frac{T(t,\boldsymbol{x}_p) - \theta_p}{\tau_{\theta,p}}, \tag{4}$$

where $\boldsymbol{x}_p(t)$, $\boldsymbol{v}_p(t)$, and $\theta_p(t)$ are position, velocity and temperature of the p-th particle, respectively. Here τ_p and τ_θ are the momentum and thermal relaxation times, given by

$$\tau_p = \frac{2}{9}\frac{\rho_p}{\rho_0}\frac{R^2}{\nu}, \qquad \tau_\theta = \frac{1}{3}\frac{\rho_p c_{pp}}{\rho_0 c_{p0}}\frac{R^2}{\kappa}, \tag{5}$$

where R, ρ_p, and c_{pp} are the radius, density and specific heat of particles. This particle representation is appropriate when particle size is much smaller than all dynamically significant flow length scales, i.e. much smaller than the Kolmogorov length scale, and particle density is much higher than fluid density, so that all other contributions to the force on particles other than the Stokes drag can be neglected (see [12]), conditions which are met in many applications where liquid or solid particles are suspended in gases.

2.2 Flow configuration

We consider the heat transfer between two regions with different temperatures T_1 and T_2, uniform within each region, within a homogeneous and isotropic velocity field which is kept statistically steady by the body force $\boldsymbol{f}_u$. The initial temperature step generates a temperature mixing layer which thickens with time. In this situation, two highly intermittent sub-layers bounding a well mixed central part of the mixing layer between the two regions emerge [13]. While velocity fluctuations are statistically steady due to the presence of the forcing, from the point of view of the temperature field, this is a transient problem, where we observe the evolution of the initial step of temperature.
We solve the problem (1-4) in a parallelepiped domain with size L_1, $L_2 = L_1$, and L_3 in directions x_1, x_2 and x_3. The initial temperature is initially equal to T_1 in the $x_3 < L_3/2$ half domain and initially equal to T_2 in the $x_4 > L_3/2$ half domain. Periodic boundary conditions are applied in all directions. In order to simulate in a consistent way a single temperature mixing layer, the temperature field is decomposed as

$$T(t,\boldsymbol{x}) = T_1 - \Gamma x_3 + T_*(t,\boldsymbol{x}) \tag{6}$$

where $\Gamma = (T_2 - T_1)/L_3$. Analogously, the particle temperature is decomposed as

$$\theta_p(t) = T_1 - \Gamma x_{p,3}(t) + \theta_p^*(t). \tag{7}$$

In this way, we can apply periodicity to T_* and θ_p^*. With this decomposition, equations 3 and 4 are modified into

$$\partial_t T_* + \boldsymbol{u}\cdot\nabla T_* = \Gamma u_3 + \kappa\nabla^2 T_* + \frac{1}{\rho_0 c_p} C_T + f_T, \tag{8}$$

$$\frac{\mathrm{d}\theta_p^*}{\mathrm{d}t} = \Gamma v_{p,3} + \frac{T_*(t,\boldsymbol{x}_p) - \theta_p^*}{\tau_{\theta,p}}. \tag{9}$$

The equations are made dimensionless by using the shorter size of the domain L_1 over 2π as a lengthscale, a velocity scale derived from the imposed kinetic energy dissipation ε, and the temperature difference $T_1 - T_2$ between the two regions as a temperature scale. Thus, the dimensionless domain has a $2\pi \times 2\pi \times 2n\pi$ size, where n is the aspect ratio of the domain. A sketch of the flow configuration can be inferred from figure 1, where the domain has an aspect ratio equal to 2. The carrier flow field equations are solved by means of a pseudo-spectral Fourier method for the spatial discretization, dealiased by means of the $3/2$ rule. Forcing is applied of a single wave-number, i.e. to all wave-vectors with the same modulus, $||\boldsymbol{k}|| = k_f$, by means of a so called deterministic largescale forcing [6, 10], which in the wavenumeber space takes the form

$$\hat{\boldsymbol{f}}(t,\boldsymbol{\kappa}) = \varepsilon \frac{\hat{\boldsymbol{u}}(t,\boldsymbol{\kappa})}{\sum_{||\boldsymbol{\kappa}||=\kappa_f} ||\hat{\boldsymbol{u}}(t,\boldsymbol{\kappa})||^2} \delta(||\boldsymbol{\kappa}|| - \kappa_f), \tag{10}$$

where ε is the imposed mean dissipation and k_f is the forced wave-number. A second order exponential Runge-Kutta time integration method has been used for both fluid and particles, in order to ensure consistency between the two phases. A recent novel numerical framework [14, 15], based on inverse and forward Non-Uniform Fast Fourier Transforms with a fourth order B-spline basis, has been used to interpolate fluid velocity and temperature at particle positions and to compute particle feedback. The fluid velocity field is initialized by running a simulation of an isotropic flow with no particles until a statistically steady state is obtained. Then, the flow is seeded by randomly distributed particles and the initial temperature step is imposed. In order to avoid a discontinuity between the two halves of the domain, the step is smoothed by means of an hyperbolic tangent, in a way similar to [9, 13], i.e. the initial temperature is

$$T(0,\boldsymbol{x}) = T_1 + \frac{T_2 - T_1}{2}\left[1 + \tanh\left(a\frac{x_3 - L_3/2}{L_3/2}\right)\right], \tag{11}$$

where coefficient a is chosen such as to smooth the step over a few grid sizes and thus to avoid the Gibbs phenomenon when the discrete Fourier transform is carried out. Initial particle velocity and temperature have been assumed equal to those of the carrier fluid at particle position. As regards temperature, this is equivalent to assume that particles have resided in the uniform temperature regions enough to reach thermal equilibrium with the carrier flow.

Table 1 – Dimensionless flow parameters for the numerical simulation.

Simulation		S1	S2	S3	S4
Taylor Reynolds number	Re_λ	37	56	86	124
Prandtl number	Pr	0.71	0.71	0.71	0.71
Dissipation rate	ε	0.25	0.25	0.25	0.25
Forced wavenumber	k_f	3	5	$\sqrt{6}$	$\sqrt{3}$
Kolmogorov length scale	η	0.041	0.0153	0.0153	0.0153
Kolmogorov time scale	τ_η	0.188	0.098	0.098	0.098
Taylor micro-scale	λ	0.51	0.226	0.29	0.35
Integral length scale	ℓ	0.72	0.40	0.74	0.94
Root mean square velocity	u'	0.64	0.59	0.71	0.85
Resolution	$\Delta x/\eta$	1.2	1.6	1.6	1.6

Table 2 – Particle parameters in dimensionless code units.

Particle volume fraction	φ	2×10^{-5}
Density ratio	ρ_p/ρ_0	10^3
ratio	St_θ/St	0.5 ; 1 ; 2 ; 3 ; 4 ; 4.43
Stokes number	St	0.1 ; 0.2 ; 0.3 ; 0.5 ; 0.7 ; 0.8 ; 0.9 ; 1 ; 1.2 ; 1.5 ; 2 ; 2.5 ; 3

2.3 Flow parameters

We simulated the heat transfer in this particle-laden flow at four Taylor microscale Reynolds numbers, ranging from 37 to 124. This has been obtained by varying the grid resolution and the wave number at the forcing is applied. The main parameters of the simulations are listed in table 1. Therefore, all simulations are in the low to moderated Reynolds number, but since the mixing of a scalar through a sharp interface is mainly driven by the large-scales of the flow [[13]], these Reynolds numbers should be high enough to quantify the heat transfer between the two homogeneous regions in a developed turbulent flow. In order to allow the temperature mixing layer to develop without being confined by the domain, an aspect ratio from 2 to 3 of the domain has been used, that is, the dimensionless domain is 2π in directions x_1 and x_2 but 4π or 6πin direction x_3. Therefore, the parallelepiped domain has been discretized with $128^2\times384$ grid points at $\mathrm{Re}_\lambda=37$ and with $256^2\times512$ grid points at higher Reynolds numbers, with the same resolution in all directions. Since the code is dealiased through the 3/2 rule, this implies that the maximum simulated wave-number is $N/2$ and not $N/3$, where N is the number of points in x_1 and x_2 directions. Note that all convective terms and fluid interpolation at particle position is computed on the finer grid used to avoid aliasing, i.e. on a $192^2\times576$ grid at $\mathrm{Re}_\lambda=37$ and $384^2\times768$ grid at higher Reynolds numbers. A particle volume fraction $\varphi=2\times10^{-5}$ is used in all simulations. Two-way coupling is more appropriate at such a volume fraction [16], but, not considering collisions, particles behave independently one from each other and one-way coupling simulations are possible; the relatively high volume fraction allows just for a larger statistical ensemble of particles, it is not meant to represent such a particle concentration.

Particle inertia in a turbulent flow is measured through the Stokes number $St=\tau_p/\tau_\eta$, which compares the particle momentum relaxation time τ_p to the Kolmogorov time scale τ_η, while, analogously, particle thermal inertia is measured through the thermal Stokes number $St_\theta=\tau_\theta/\tau_\eta$. The ratio $St_\theta/St=(3/2)(c_{pp}/c_{p0})\mathrm{Pr}$, that is the ratio between the momentum and thermal relaxation times, depends only of the thermal properties of the carrier fluid and suspended particles. For example, in air this ratio is between 0.5 and 1 for metallic particles and soot, while is it around 2 for organic material particles, like wood or oils, slightly above two for ice particles and around 4.43 for pure water. Therefore, we have carried out a set of simulations which cover a wide range of St_θ/St, between 0.5 and 4.43, with a Prandtl number equal to 0.71, which is representative of particles suspended in air.

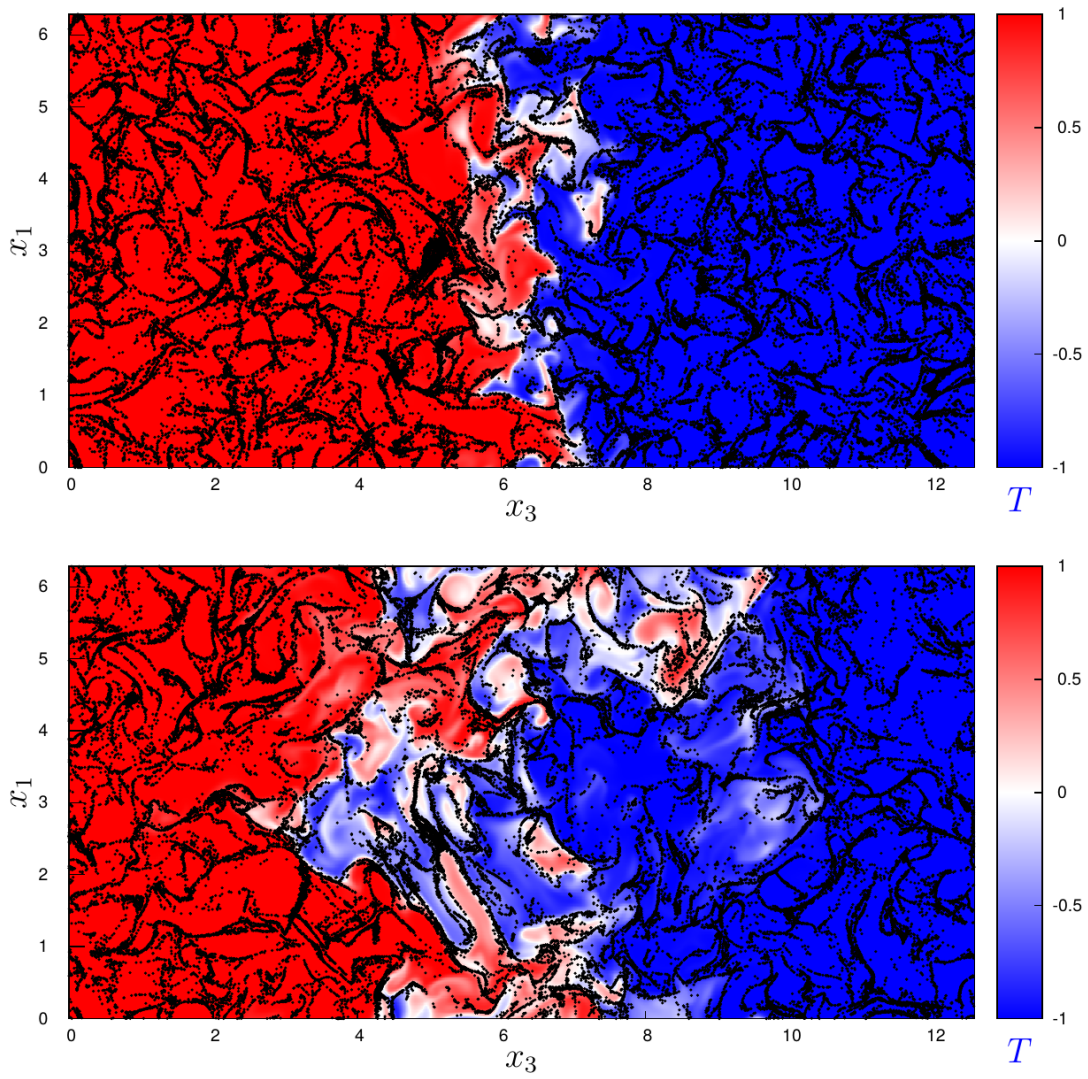

Figure 1 – Visualization of the dimensionless fluid temperature $t/\tau = 3$ in a simulation with $\mathrm{Re}_\lambda = 56$ (top), and $\mathrm{Re}_\lambda = 124$ (bottom) $\mathrm{Pr} = 0.71$. Particle volume fraction is 2×10^{-5} with $St = 1$ and $\mathrm{St}_\vartheta/\mathrm{St} = 4.43$.

2.4 Averages

The velocity field is homogeneous and isotropic, while the temperature field in homogeneous only in directions x_1 and x_2. Therefore, all averages are taken as plane averages on (x_1, x_2) planes. The average on particles have been computed by considering only particles whose position in x_3 direction lays between $x_3 - \Delta x$ and $x_3 + \Delta x$, where Δx is the grid spacing in physical space. Since the temperature field is unsteady, no time average is possible. All simulations have been repeated three times by using uncorrelated different initial velocity fields in order to increase the ensemble and thus obtain more accurate statistics.

3. Results and discussion

A visualization of the temperature field is shown in figure 1. The temperature interface, which initially separates the two regions at uniform temperature, is spread by turbulent eddies and a mixing region with high temperature variance is generated.

The width of the mixing region can be measured by considering the mean temperature distribution of the carrier flow (Fig. 2(a)): we define the temporal mixing layer thickness δ as

$$\delta(t) = \frac{T_1 - T_2}{\max\left\{\left|\frac{\partial \langle T \rangle}{\partial x_3}\right|\right\}} \tag{12}$$

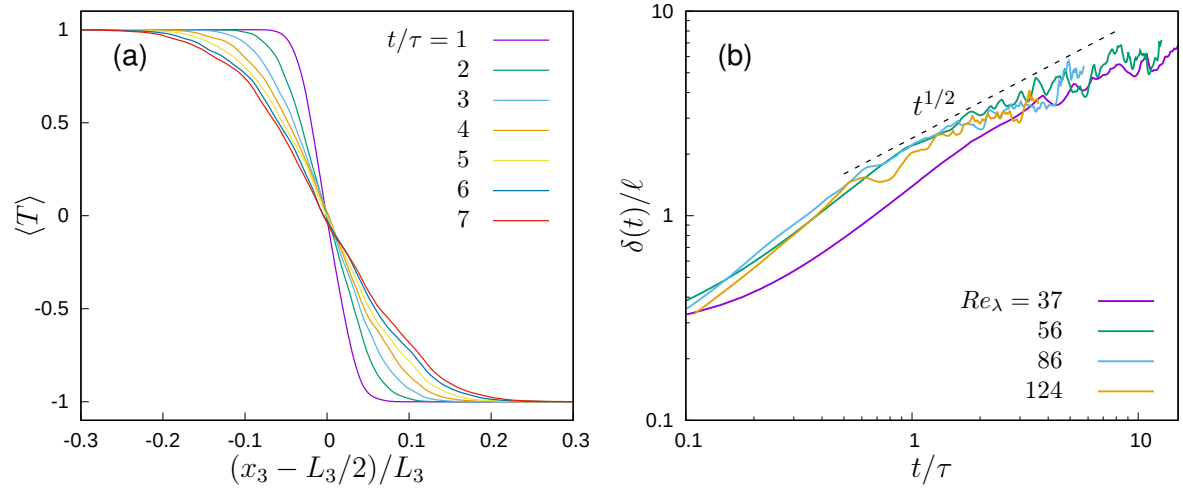

Figure 2 – (a) Time evolution of the dimensionless mean fluid temperature at $\mathrm{Re}_\lambda = 56$; (b) growth of the mixing layer thickness in one-way coupling simulations for different Re_λ.

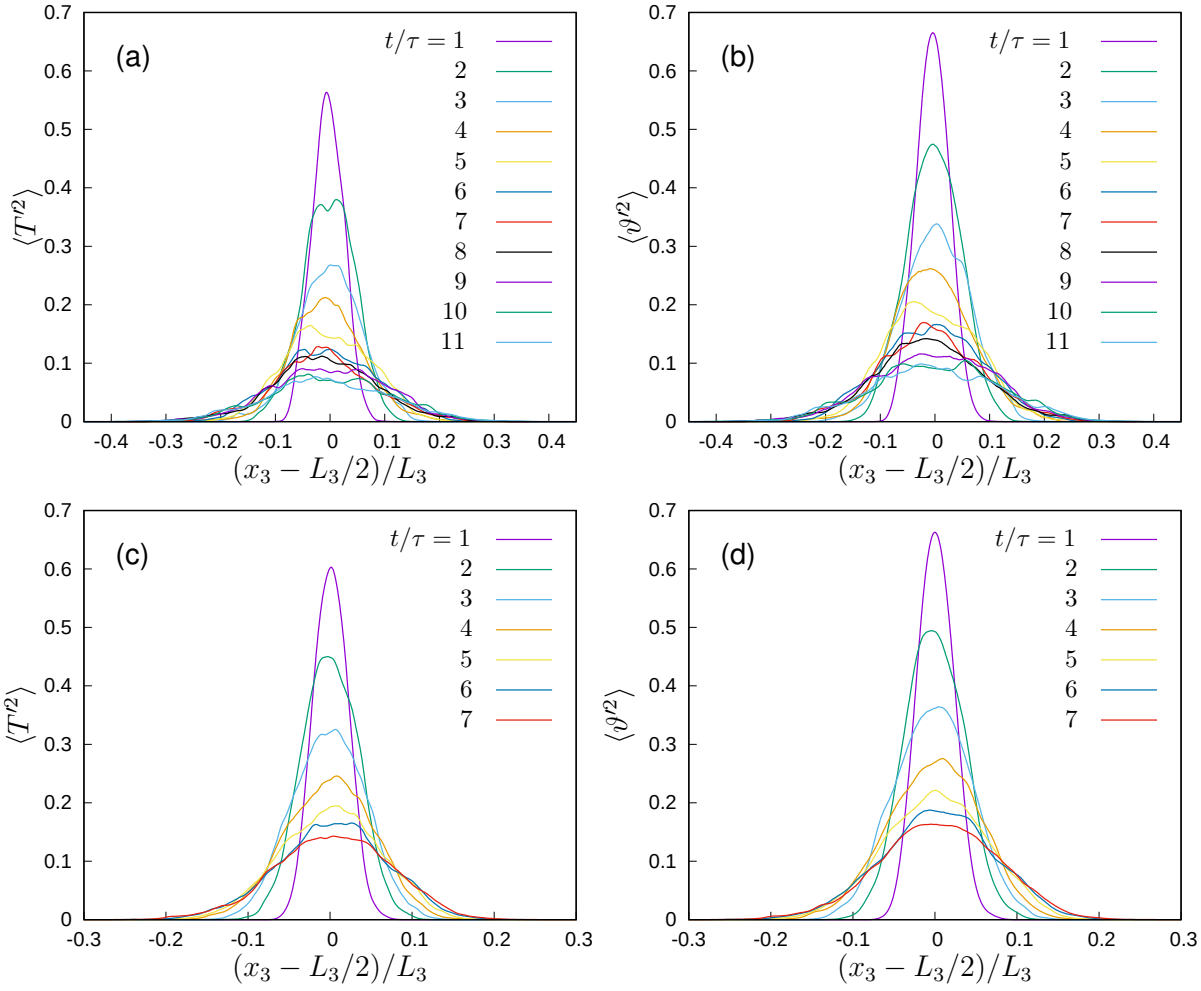

Figure 3 – Time evolution of (a) the fluid temperature variance (b) the particle temperature variance at $\mathrm{Re}_\lambda = 37$ and time evolution of (c) the fluid temperature variance and (d) the particle temperature variance at $\mathrm{Re}_\lambda = 56$ (one-way coupling simulations at $\mathrm{St} = 1.0$ and $\mathrm{St}_\vartheta/\mathrm{St} = 4.43$).

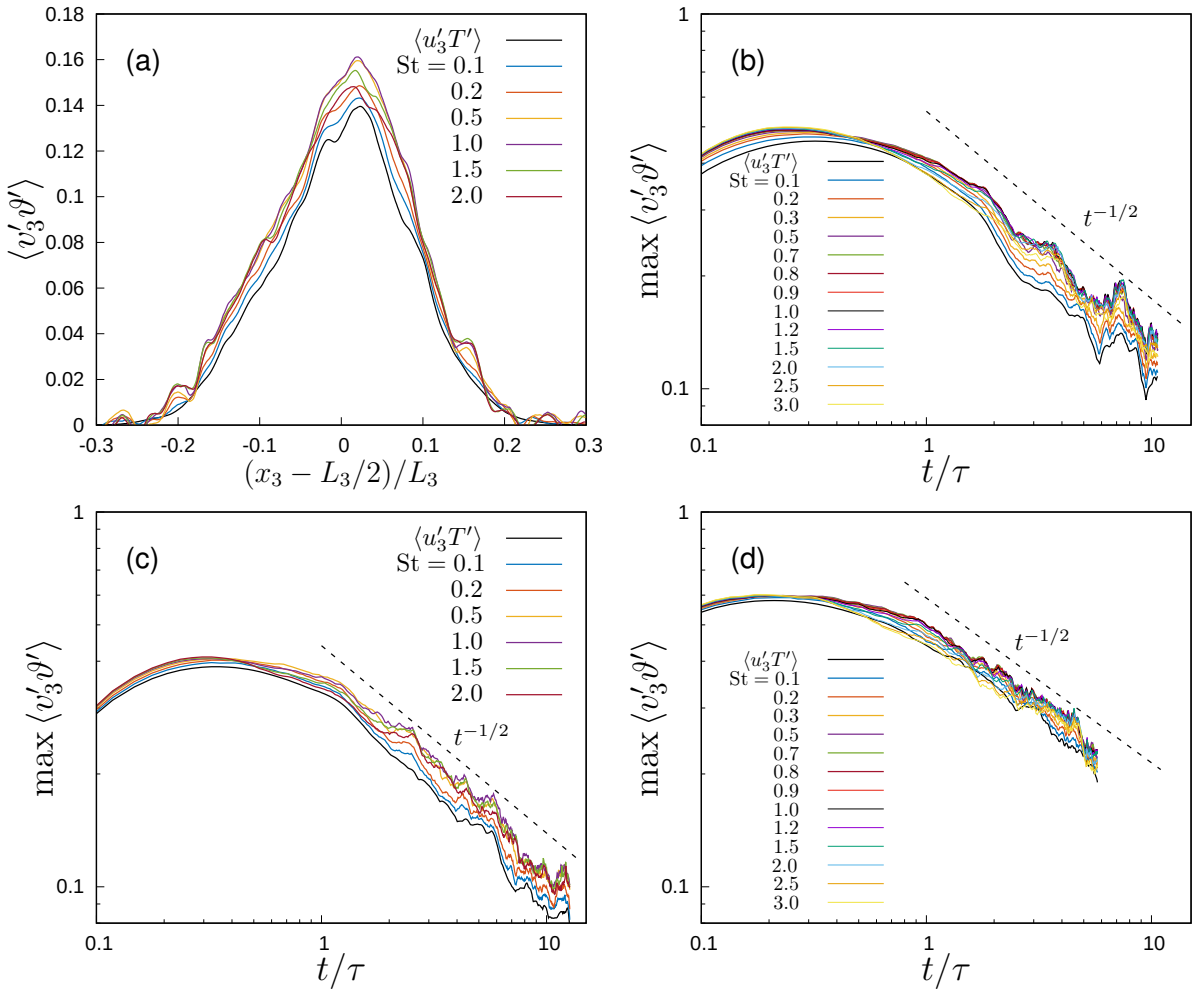

Figure 4 – Spatial distribution of (a) velocity and temperature correlation at $t/\tau = 6$ and $\mathrm{Re}_\lambda = 56$ and the maximum heat flux of carrier flow field for (b) $\mathrm{Re}_\lambda = 37$, (b) $\mathrm{Re}_\lambda = 56$ and (d) $\mathrm{Re}_\lambda = 86$ (all for different Stokes number in one-way coupling simulations at $\mathrm{St}_\vartheta/\mathrm{St} = 4.43$)

This definition is different from the one used in shearless mixings, but it has the advantage to be independent from the shape of the mean temperature profile and to not involve any arbitrary definition of the border of the layer. The mixing layer thickness shows an almost diffusive $t^{1/2}$ growth (Fig. 2(b)) after an initial transient of about one eddy turnover time ℓ/u', in agreement with the studies on the spreading of shearless mixings in a decaying turbulence (e.g. [13]). The initial growth at the lowest Reynolds number is slower but this simulation had a slightly different initial temperature profile due to the coarser resolution. Anyway, it still reaches the $t^{1/2}$ growth regime. After the initial transient before a $t^{1/2}$ growth of δ is achieved, during which velocity-temperature correlations are created and particles cluster according to their inertia, a self-similar stage of evolution is observed, during which all single-point statistics of the carrier fluid and the suspended particles collapse when properly rescaled. This implies that position has to be normalized with the thickness $\delta(t)$, while the variance of temperature fluctuations and the correlation between temperature and correlation with the inverse of $\delta(t)$ (see figures 3 and 4).

The correlations between temperature and velocity fluctuations is the most important result because it is proportional to the heat transfer between the two flow regions at different temperature, whose quantification is our main aim. The heat flux $\dot{q}$ in the direction of the temperature inhomogeneity x_3 can be decomposed into the contribution of: thermal diffusion, convection by fluid velocity and transport associated with the particle motion. All these contributions are maximum in the centre of the domain, i.e. at the position of the initial temperature step, and, in the self-similar stage, reduce in time as $t^{-1/2}$ while the mixing layer grows and the driving mean temperature gradient reduces.

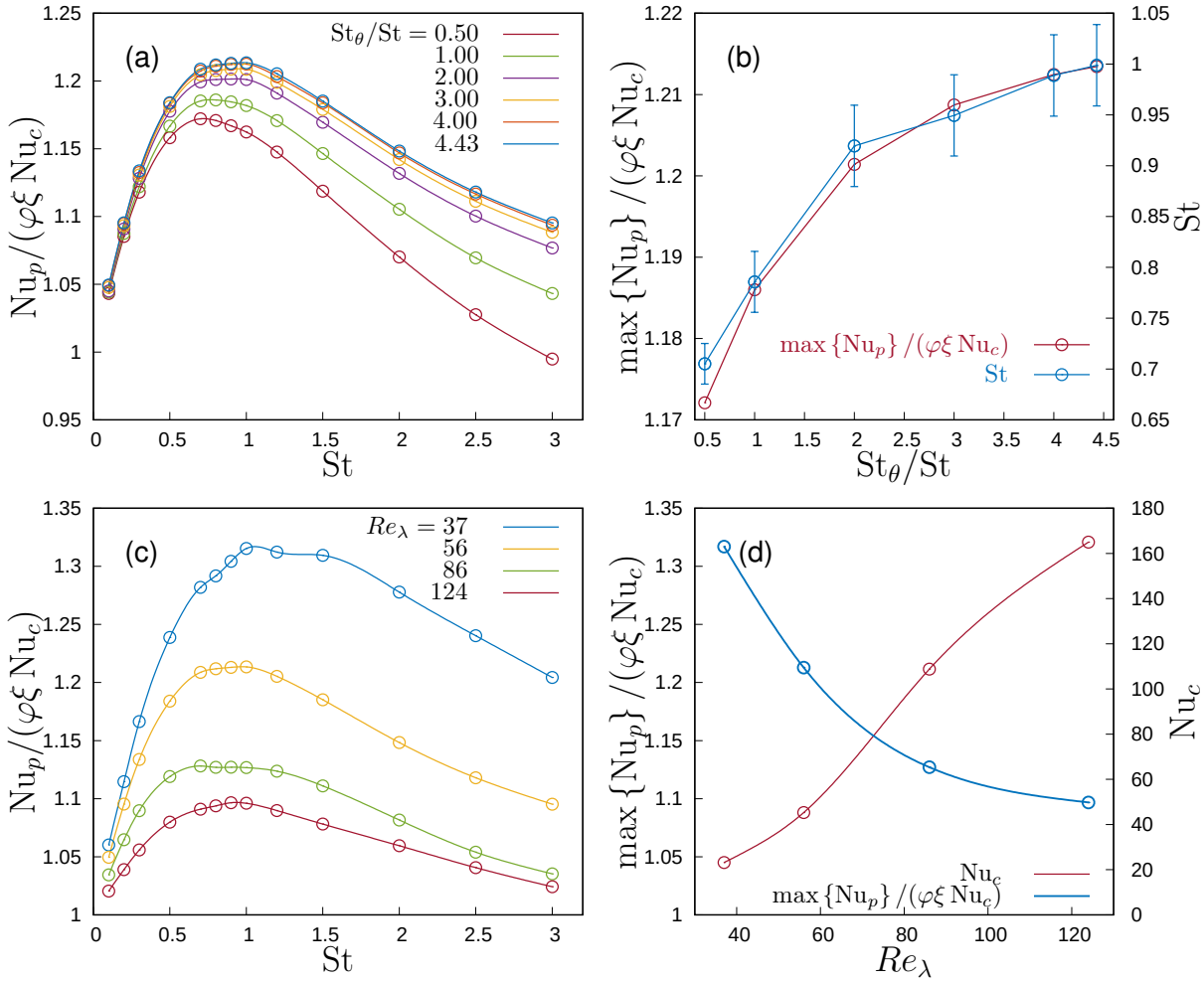

Figure 5 – (a) Particle motion contribution to the Nusselt number, Nu_p as a function of the Stokes number in one-way coupling regime; Nu_c is the fluid convection contribution to the Nusselt Number, φ the volume fraction and $\xi = \rho_p c_{pp}/(\rho_0 c_{p0})$ is the ratio between particle and fluid specific heat capacities. (b) The maximum Nusselt number and its corresponding Stokes number for each thermal Stokes number and Stokes number ratio. (c) Particle motion contribution to the Nusselt number, Nu_p as a function of the Stokes number and Reynolds number. (d) variation of convective Nusselt number in terms of Taylor Reynolds number Re_λ

Inertial particles can carry large temperature differences at long distances, therefore they can give a significant contribution to the heat transfer.

To quantify the effect of each parameter on the heat transfer we use the Nusselt number, Nu, customary defined as the ratio of the heat transfer to the thermal diffusion. By using as a length-scale the mixing thickness $\delta(t)$, which is the only length-scale dynamically significative for the heat transfer in the present flow configuration, the Nusselt number remains constant in the self-similar stage of evolution of the mixing. By using standard dimensional analysis, the Nusselt number Nu, ratio between the heat transfer and the diffusive heat transfer, can be written as

$$\mathrm{Nu} = \mathrm{Nu}(\mathrm{Re}, \mathrm{Pr}, \mathrm{St}, \mathrm{St}_\vartheta) \tag{13}$$

The heat flux per unit surface and unit time is given by the sum of heat flux due to diffusion, convection and particle motions, $\dot{q} = \dot{q}_d + \dot{q}_c + \dot{q}_p$, where, from equations (1-4),

$$\dot{q}_d = -\lambda \frac{\partial \langle T \rangle}{\partial x_3}, \tag{14}$$

$$\dot{q}_c = \rho_0 c_{p0} \langle u_3' T' \rangle, \tag{15}$$

$$\dot{q}_p = \varphi \rho_p c_p \langle v_3' \theta' \rangle. \tag{16}$$

herefore, the Nusselt number can be written as

$$\mathrm{Nu} = 1 + \mathrm{Nu}_c + \mathrm{Nu}_p \tag{17}$$

where Nu_c and Nu_p are the convective and particle contributions, given by

$$\mathrm{Nu}_c = \mathrm{RePr}\frac{-\langle\tilde{u'}_3\tilde{T}'\rangle}{\partial\langle\tilde{T}\rangle/\partial\tilde{x}_3}, \tag{18}$$

$$\mathrm{Nu}_p = \varphi\mathrm{RePr}\frac{\rho_p c_{pp}}{\rho_0 c_{p0}}\frac{-\langle\tilde{v'}_3\tilde{\theta}'\rangle}{\partial\langle\tilde{T}\rangle/\partial\tilde{x}_3} == \varphi\mathrm{RePr}\xi\frac{-\langle\tilde{v'}_3\tilde{\theta}'\rangle}{\partial\langle\tilde{T}\rangle/\partial\tilde{x}_3} \tag{19}$$

Here, the tilde indicates dimensionless variables, the apex indicate fluctuations, and coefficient $\xi = (\rho_p c_{pp})/(\rho_0 c_{p0})$ is the ratio between the specific heat capacities of the particles and the carrier fluid. In the one-way coupling regime, the carrier fluid temperature is not modified by the presence of particles, therefore the convective heat flux depends only on fluid properties and on the underlaying turbulence, so that $\mathrm{Nu}_c = \mathrm{Nu}_c(\mathrm{Re},\mathrm{Pr})$. The dependence of the convective Nusselt number on Reynolds number is shown in figure 5(d). Analogously, particle velocity and temperature in the one-way coupling regime depend on the Stokes and thermal Stokes number but particles do not interact in any way, directly or indirectly through the carrier fluid, so that $\langle v'_3\vartheta'\rangle$ are not affected by particle density and, as a consequence, $\mathrm{Nu}_p = \varphi\mathrm{RePr}\xi f(\mathrm{St},\mathrm{St}_\vartheta)$. Therefore in the one-way coupling regime, only Nu_p is affected by particle inertia and thermal inertia, and $\mathrm{Nu}_p/\mathrm{Nu}_c$ is a useful indicator of the enhancement of the heat transfer due to the presence of particles. We remark that the existence of a self-similar stage implies that the Nusselt number does not depend on time, since all fluxes have the same temporal evolution. The heat flux between is evaluated at the centre of the domain, i.e. at the plane initially separating the two regions, which is also where the gradient of the mean temperature of the carrier fluid is maximum. Figure 5(a) shows the particle contribution of particle motion to the Nusselt number as a function of the Stokes number in the one-way coupling regime for different ratios between thermal Stokes number and Stokes number at fixed Reynolds number, $\mathrm{Re}_\lambda = 56$, while figure 5(c) shows the particle contribution to the Nusselt number for different Reynolds numbers but for a fixed thermal Stokes to Stokes number ratio $\mathrm{St}_\vartheta/\mathrm{St} = 4.43$. When the Stokes number approaches zero particles behave as passive tracers and, since also the thermal Stokes number approaches zero, they tend to be also in thermal equilibrium with the local carrier fluid, thus $\mathrm{Nu}_p \to \varphi\xi\mathrm{Nu}_c$ in this limit. The heat flux has a maximum when the Stokes number approaches one, a situation which corresponds to the maximum clustering of particles. In the investigated ranges of $\mathrm{St}_\vartheta/\mathrm{St}$, this maximum is not achieved at $\mathrm{St} = 1$, but at a smaller Stokes number, which increases with $\mathrm{St}_\vartheta/\mathrm{St}$, from around 0.6 when $\mathrm{St}_\vartheta/\mathrm{St} = 0.5$ increasing to almost 1 when $\mathrm{St}_\vartheta/\mathrm{St} = 4.43$, as it is shown in figure 5(b) for the simulation at $\mathrm{Re}_\lambda = 56$. This trend is present at all Reynolds numbers, suggesting that the maximum heat transfer due to particles is achieved at $\mathrm{St} = 1$ only in the asymptotic limit for $\mathrm{St}_\vartheta/\mathrm{St} \to \infty$. The maximum increases monotonically with the $\mathrm{St}_\vartheta/\mathrm{St}$ ratio, which makes particles with high thermal capacities able to significantly increase the heat flux. However, since the ratio $\xi = (\rho_p c_{pp})/(\rho_0 c_{p0})$ can easily be of order $10^3 \div 10^4$ for liquid or solid particles in a gas, the presence of particles can significantly enhance the overall heat flux even at moderate concentrations. It is evident, however, that the heat transfer enhancement due to particles is much more strongly affected by St than by St_ϑ alone, as indicated by the data in figure 5(a,c). Indeed, in the investigated range of particle to fluid thermal capacity ratio, the maximum particle Nusselt number changes by around 5% for the same Reynolds number. For $\mathrm{St} \gtrsim 1$ the particle velocity dynamics becomes increasingly non-local, reducing clustering and the heat flux. From the investigated range of Stokes number it is not possible to infer an asymptotic limit for $\mathrm{St} \to \infty$. However, in such a limit particle dynamics becomes uncorrelated from the dynamics of the carrier fluid, therefore their dynamics can be only determined by particle collisions and one can expect that, in such condition, particles behave like molecules and therefore the heat transport approaches a diffusive limit, leading again to $\mathrm{Nu}_p/(\varphi\xi\mathrm{Nu}_c) \to 1$. This is compatible with present simulations. The rate of approach to such a limit appear to depend, however, from the $\mathrm{St}_\vartheta/\mathrm{St}$ ratio, and is significantly slower for high values of $\mathrm{St}_\vartheta/\mathrm{St}$.

It should be noted that, unlike the Rayleigh-Bénard problem analysed by Park et al. [17], the effect of preferential concentration and clustering exhibits itself not only in the thermal coupling, but already in the one-way regime in absence of any modulation of the carrier flow by particles.

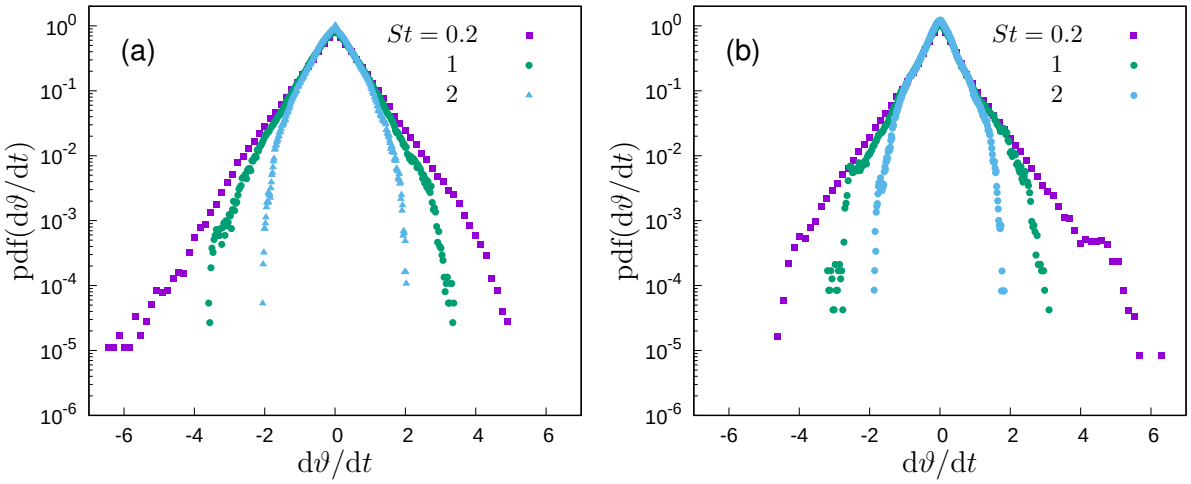

Figure 6 – Probability density function of the particle temperature derivative at $t/\tau = 4$: (a) simulation at $\mathrm{Re}_\lambda = 56$, (b) simulation at $\mathrm{Re}_\lambda = 86$.

Anyway, when the Reynolds number is increased, particle Nusselt number increases less than the convective Nusselt number, so that the ratio $\mathrm{Nu}_p/\mathrm{Nu}_c$ reduced (see figure 5, panels (c) and (d)). By fitting the data in figure 5(d), one can infer that the maximum particle Nusselt number scales as

$$\max_{\mathrm{St}}\{\mathrm{Nu}_p\} \sim \varphi \mathrm{Nu}_c \left(1 + 12\,\mathrm{Re}_\lambda^{-1}\right) \tag{20}$$

We expect these findings to hold, at least qualitatively, also in the two-way coupling regime. However, since inertial particles tend to preferentially concentrate in the advected scalar fronts, where the gradient of temperature is large, they act to smooth the temperature gradients, therefore we expect that particle thermal feedback would lead to a potential reduction of the overall heat flux.
The probability density function of the particle temperature derivative is shown in figure 6 at Re_λ equal to 56 and 86 for three Stokes number when $\mathrm{St}/\mathrm{St}_\vartheta = 4.43$ in the central region of the temperature mixing layer at $t/\tau = 4$, that is, during the self-similar stage of evolution. It is possible to observe that the shape of this probability density function depends on the particle inertia: when the Stokes number increases, the probability density function becomes narrower. This can be explained by observing that, as the Stokes number increases, particles are slower to respond to changes in the temperature field, producing and effect which is analogous to the observed filtering of velocity due to their inertia. This implies that, extreme derivatives of the temperature are unlikely to be present at higher inertia, even if the particle temperature can differ strongly form the local temperature of the carrier flow. Therefore, intermittency of particle temperature, as measured by the kurtosis, reduces with the Stokes number. This behaviour is qualitatively analogous of what has been observed in homogeneous and isotropic turbulence [10], suggesting that, in the self-similar stage, which is reached in only about one eddy turnover time, the temperature statistics approach the ones in a homogeneous flow.

3.1 Implications for turbulence modelling

Results of simple flow configuration where all parameters can be independently varied are useful as a benchmark to validate and improve existing RANS or LES models which include heat transfer. As regards RANS modelling, in the present flow configuration it is immediate to deduce the model consistency and model coefficients. As an example, we can use a $k-\varepsilon$ eddy diffusivity model, even if it tends to perform quite poorly in unconfined flows. In such an approach, the heat transport due to turbulent fluctuations $-\rho_0 c_{p0}\langle\vartheta'\boldsymbol{u}'\rangle$ is modelled as $-\rho_0 c_{p0}\kappa_T\nabla\langle T\rangle$ through the introduction of a thermal eddy diffusivity is $\kappa_T = \nu_T/\mathrm{Pr}_T$, where $\nu_T = c_\mu k^2/\varepsilon$ is the eddy kinematic viscosity, c_μ a model coefficient, and Pr_T a so-called turbulent Prandtl number, which is another model coefficient. In present flow, since the velocity field is statistically steady and homogeneous, ν_T is constant both in space and time, and, as a consequence, also κ_T if a constant turbulent Prandtl number is assumed.

This leads to a $t^{1/2}$ growth of the temperature mixing layer thickness and a $t^{-1/2}$ reduction of the heat flux, which is consistent with the results of present simulations. More specifically, in such a case $\delta(t) = 2\sqrt{\pi(\kappa+\kappa_T)t} \simeq 2\sqrt{\pi\kappa_T t}$, when the same definition of δ introduced in (12) is used, while $\mathrm{Nu}_c = \kappa_T/\kappa$, so that it is possible to infer the value of κ_T, and therefore the model coefficient c_μ/Pr_T, from simulations. From the data in figures 2 and 5(d) we can conclude that c_μ/Pr_T is between 0.13 and 0.21, depending on the Reynolds number. This is up to 0.5 times higher than the expected value by using the most common coefficients, $c_\mu = 0.09$ and $\mathrm{Pr}_T = 0.6$. The discrepancy can be due to the moderate Reynolds number of the simulation but can also indicate a limitation of the model when there is no shear.

When particles are represented as a continuum phase in an Eulerian-Eulerian modelling approach, they are described by a particle number density, a particle mean velocity $\boldsymbol{v}$ and a particle mean temperature ϑ fields, which are a function of space and time. By carrying out RANS averages one would need to model the turbulent heat fluxes as well, which, in the eddy diffusivity framework, would imply to write $-\langle\vartheta'\boldsymbol{v}'\rangle$ as $-\kappa_T^*\nabla\langle\vartheta\rangle$. In the flow we simulated, our result would imply that κ_T^* is constant. Since $\kappa_T^*/\kappa_T = \mathrm{Nu}_p/(\varphi\xi\mathrm{Nu}_c)$, the data presented in previous section (in particular in panels (a) and (c) of figure 5) allow to deduce κ_T^* from the local Reynolds number and particle Stokes and thermal Stokes numbers. A fitting of the curves shown can produce the required model.

A similar analysis can be carried out for any model and also for LES models, even if in such a case the heat transport cannot be immediately deduced from the model but requires to perform LES simulations.

Acknowledgements

The authors acknowledge the CINECA award IsC85_PATTI under the ISCRA initiative, for the availability of high performance computing resources and support.

4. Contact Author Email Address

Authors' email: hamid.zandipour@polito.it, michele.iovieno@polito.it.

5. Copyright Statement

References

[1] Brandt L and Coletti F. Particle-laden turbulence: Progress and perspectives. *Annual Review of fluid Mechanics*, Vol. 54, pp. 159–189, 2022.

[2] Elgobashi S. Direct numerical simulation of turbulent flows laden with droplets or bubbles. *Annual Review of fluid Mechanics*, Vol. 51, pp. 217–244, 2019.

[3] Zonta F, Marchioli C, and Soldati A. Direct numerical simulation of turbulent heat transfer modulation in micro-dispersed channel flow. *Acta Mechanica*, Vol. 195, No. 1–4, pp. 305–326, 2008.

[4] Kuerten J G M, van der Geld C W M, and Geurts B J. Turbulence modification and heat transfer enhancement by inertial particles in turbulent channel flow. *Physics of Fluids*, Vol. 23, No. 12, art. no. 123301, 2011.

[5] Zamansky R, Coletti F, Massot M, and Mani A. Turbulent thermal convection driven by heated inertial particles. *J. Fluid Mech.*, Vol. 809, pp. 390–437, 2016.

[6] Kumar B Schumacher J and Shaw R A. Cloud microphysical effects of turbulent mixing and entrainment. *Theoretical and Computational Fluid Dynamics*, Vol. 27, No. 3, pp. 361–376, 2013.

[7] Kumar B Schumacher J and Shaw R A. Lagrangian mixing dynamics at the cloudy–clear air interface. *J.Atmos. Sci.*, Vol. 71, No. 7, pp. 2564–2580, 2014.

[8] Götzfried P, Kumar B, Shaw R A, and Schumacher J. Droplet dynamics and fine-scale structure in a shearless turbulent mixing layer with phase changes. *Journal of Fluid Mechanics*, Vol. 814, pp. 452–483, 2017.

[9] Bhowmick T and Iovieno M. Direct numerical simulation of a warm cloud top model interface: Impact ofthe transient mixing on different droplet population. *Fluids*, Vol. 4, No. 3, art. no. 144, 2019.

[10] Carbone M, Bragg A D, and Iovieno M. Multiscale fluid–particle thermal interaction in isotropic turbulence. *Journal of Fluid Mechanics*, Vol. 881, pp. 679–721, 2019.

[11] Saito I, Watanabe T, and Gotoh T. Modulation of fluid temperature fluctuations by particles in turbulence. *Journal of Fluid Mechanics*, Vol. 931, art. no. A6, 2022.

[12] Maxey M R and Riley J J. Equation of motion for a small rigid sphere in a nonuniform flow. *Physics of Fluids*, Vol. 26, No. 4, pp. 883–889, 1983.

[13] Iovieno M, Di Savino S, Gallana L, and Tordella D. Mixing of a passive scalar across a thin shearless layer: concentration of intermittency on the sides of the turbulent interface. *Turbulence*, Vol. 15, No. 5, pp. 311–334, 2014.

[14] Carbone M and Iovieno M. Application of the non-uniform fast fourier transform to the direct numerical simulation of two-way coupled turbulent flows. *WIT Transactions on Engineering Sciences*, Vol. 120, pp. 237–248, 2018.

[15] Carbone M and Iovieno M. Accurate direct numerical simulation of two-way coupled particle-laden flows through the nonuniform fast fourier transform. *Int. J. Safety and Sec. Eng.*, Vol. 10, No. 2, pp. 191–200, 2020.

[16] Elghobashi S. Particle-laden turbulent flows: direct simulation and closure models. *Applied Scientific Research*, Vol. 48, No. 3, pp. 301–314, 1991.

[17] Park H J, O'Keefe K, and Richter D H. Rayleigh-Bénard turbulence modified by two-way coupled inertial, nonisothermal particles. *Phys. Rev. Fluids*, Vol. 3, art. no. 034307, 2018.